

Protein-Templated Ugi Reactions versus In-Situ Ligation Screening: Two Roads to the Identification of SARS-CoV-2 Main Protease Inhibitors

Rebekka Wamser,^[a] Xinting Zhang,^[a] Benno Kuroepka,^[b] Christoph Arkona,^[a] and Jörg Rademann^{*[a]}

Protein-templated fragment ligation was established as a method for the rapid identification of high affinity ligands, and multicomponent reactions (MCR) such as the Ugi four-component reaction (Ugi 4CR) have been efficient in the synthesis of drug candidates. Thus, the combination of both strategies should provide a powerful approach to drug discovery. Here, we investigate protein-templated Ugi 4CR quantitatively using a fluorescence-based enzyme assay, HPLC-QTOF mass spectrometry (MS), and native protein MS with SARS-CoV-2 main protease as template. Ugi reactions were analyzed in aqueous buffer at varying pH and fragment concentration. Potent inhibitors of the

protease were formed in presence of the protein via Ugi 4CR together with Ugi three-component reaction (Ugi 3CR) products. Binding of inhibitors to the protease was confirmed by native MS and resulted in the dimerization of the protein target. Formation of Ugi products was, however, more efficient in the non-templated reaction, apparently due to interactions of the protein with the isocyanide and imine fragments. Consequently, in-situ ligation screening of Ugi 4CR products was identified as a superior approach to the discovery of SARS-CoV-2 protease inhibitors.

Introduction

Protein-templated fragment ligation is an alternative to conventional high-throughput screening allowing to evolve and identify super-additive, bioactive fragment combinations from low-affinity fragments in presence of the target protein.^[1] While initially reversible ligation reactions were employed,^[2a-c] more recently the method was extended to irreversible ligation and to CC-coupling reactions.^[2d-e] As the first example of a protein-templated multicomponent reaction (MCR), the three component Mannich ligation reaction was reported catalyzed by the human transcription factor STAT5.^[3] Isocyanide-based MCR such as Passerini^[4] and Ugi reactions,^[5] as well as modifications^[6] thereof, have gained fundamental importance in drug discovery in recent years.^[5-7] Prominent products include the HIV protease inhibitor Indinavir (Crixivan) and inhibitors of SARS-CoV main proteases.^[6a,c,7-8] The Groebke-Blackburn-Bienaymé reaction was

the first isocyanide-based MCR investigated in target-guided synthesis using urokinase plasminogen activator as the protein template,^[9] however, van der Veken *et al.* did not observe the protein-templated formation of inhibitors. Hirsch *et al.* reported protein-templated Ugi four-component reactions (4CR) using the protein targets endothiapepsin and the β -sliding clamp DnaN with NMR- and HPLC-based methods, albeit without product quantification.^[10] Considering the broad relevance of Ugi 4CR in drug discovery, we decided to take a closer look at protein-templated Ugi reactions to investigate their potential in drug discovery, focusing at the quantification and kinetics of product formation.

The main protease (M^{pro}) of SARS-CoV-2, essential for viral proliferation in host cells, was selected as the target protein to investigate protein-templated Ugi 4C reactions. To get first insights, we studied the influence of common additives in enzyme-based assays on the Ugi 4CR and its side products to optimize the buffer composition under physiological conditions. Afterwards, we investigated the catalytic effect of the SARS-CoV-2 M^{pro} on the Ugi 4CR with three different methods, a fluorescence-based enzymatic assay for the detection of enhanced inhibitory activity, HPLC-QTOF-MS analysis for the quantification of formed Ugi products, and native MS for binding studies. The aim of this study was to develop a suitable screening method for fragments forming inhibitors of SARS-CoV-2 main protease in an enzyme activity assay, using the Ugi 4CR in-situ without the time-consuming step of isolation and purification of the final products.

[a] R. Wamser, X. Zhang, C. Arkona, J. Rademann
Department of Biology, Chemistry and Pharmacy, Institute of Pharmacy,
Medicinal Chemistry,
Freie Universität Berlin, Königin-Luise-Str.2 +4, 14195 Berlin, Germany
E-mail: joerg.rademann@fu-berlin.de

[b] B. Kuroepka
Department of Biology, Chemistry and Pharmacy, Institute of Chemistry and
Biochemistry,
Freie Universität Berlin, Thielallee 63, 14195 Berlin, Germany

Supporting information for this article is available on the WWW under
<https://doi.org/10.1002/chem.202303940>

© 2024 The Authors. Chemistry - A European Journal published by Wiley-VCH GmbH. This is an open access article under the terms of the Creative Commons Attribution Non-Commercial License, which permits use, distribution and reproduction in any medium, provided the original work is properly cited and is not used for commercial purposes.

Results and Discussion

Ugi reactions in aqueous buffer

Protein-templated Ugi reactions were investigated in buffer systems employed for SARS-CoV-2 protease assays targeting Ugi product **1** (Figure 1).^[8b] All starting fragments **F1–F4**, nicotinaldehyde **F1**, 4-(pyridine-2-yl)-aniline **F2**, (*S*)-(-)- α -methylbenzyl isocyanide **F3**, and furan-2-carboxylic acid **F4** were well soluble in DMSO and buffer at concentrations suitable for the enzyme assay. The IC_{50} value of isolated Ugi product **1** of 0.82 μ M was determined in an enzyme assay using the fluorogenic substrate Dabcyl-KTSAVLQ/SGFRKM-E(Edans)-amide as a FRET probe, slightly better than the reported value of 1.81 μ M (Figure 1 and Supplementary Figure 1). Inhibition of the protease by Ugi product **1** was rationalized by the binding of the 3-pyridinyl residue of aldehyde building block **F1** into the S1 pocket as a glutamine mimetic forming a hydrogen bond to His163,^[8b] in accordance with a previous study on inhibitory fragments targeting the S1 site with pyridine (Figure 1a and b).^[11] The 4-(pyridin-2-yl)-phenyl residue, originating from the amine **F2** and the (*S*)-1-phenyl-ethyl residue from the isocyanide **F3** were proposed to occupy the S2 and S3/S4

pockets, respectively, and the furyl residue of carboxylic acid **F4**, was located at the S1' site, forming a hydrogen bond to the backbone NH of Gly143.^[8a] For control, the Ugi 3CR product **2** was synthesized as well displaying an IC_{50} value of 300 μ M in the SARS-CoV-2 M^{pro} assay.^[12]

At first, the impact of the pH value on the Ugi reaction was investigated. Considering that SARS-CoV-2 M^{pro} is active in the range of pH 6.0–8.0 with an optimum at 7.0–7.5,^[13] 3-(*N*-morpholino)-propanesulfonic acid (MOPS) and 4-(2-hydroxyethyl)-1-piperazine-ethanesulfonic acid (HEPES) were employed as buffer salts at concentrations of 100 mM, typical for 3C and 3CL protease assays. EDTA was omitted from the assay composition to avoid additional carboxylates competing with fragment **F4**. All four fragments were dissolved with final concentrations of 50 mM in buffer, and after 24 h at room temperature, the reaction mixtures were analyzed by HPLC-MS to monitor product formation at 254 nm (Figure 1d and Supplementary Figure 2). In all experiments, the 4C Ugi product **1** and the 3CR Ugi product **2** were the two dominant products. Highest conversion of the starting fragments was observed at pH 6 in MOPS buffer yielding about 50% of **1** and 30% of **2**. Conversion was reduced at higher pH, for example at pH 8 in HEPES buffer. Possible reasons for the more efficient product formation at

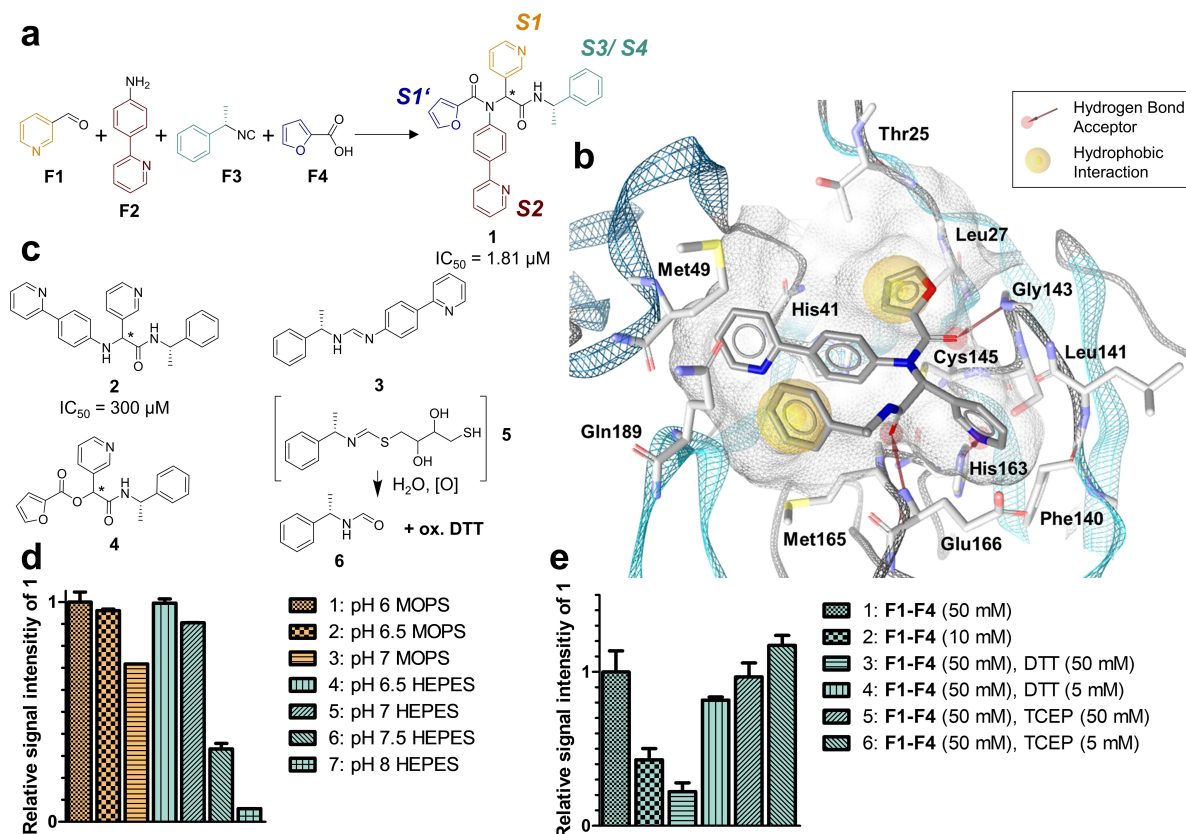


Figure 1. a. Ugi four-component reaction (Ugi 4CR) of fragments **F1–F4** yielding product **1** with annotated positions of the fragments into the S1–S4 and S1' pockets of SARS-CoV-2 M^{pro} .^[8b] b. Proposed binding mode of **1** with the SARS-CoV-2 M^{pro} . Color code: white and grey sticks – carbon atoms, yellow sticks – sulfur atoms, blue sticks – nitrogen atoms, red sticks – oxygen atoms. c. By-products observed from Ugi 4CR. d. Investigation of the Ugi 4CR in different buffers and at different pH values over 24 h at room temperature (50 mM fragment concentration). The amount of **1** was determined with the AUC from the 254 nm UV chromatogram and normalized to the highest amount of compound **1** in reaction 1. e. Impact of fragment concentration, DTT and TCEP on the formation of Ugi product **1** over 24 h at room temperature in HEPES buffer (100 mM), pH 8. The amount of **1** was determined by integration of the extracted ion chromatogram and was normalized to reaction 1.

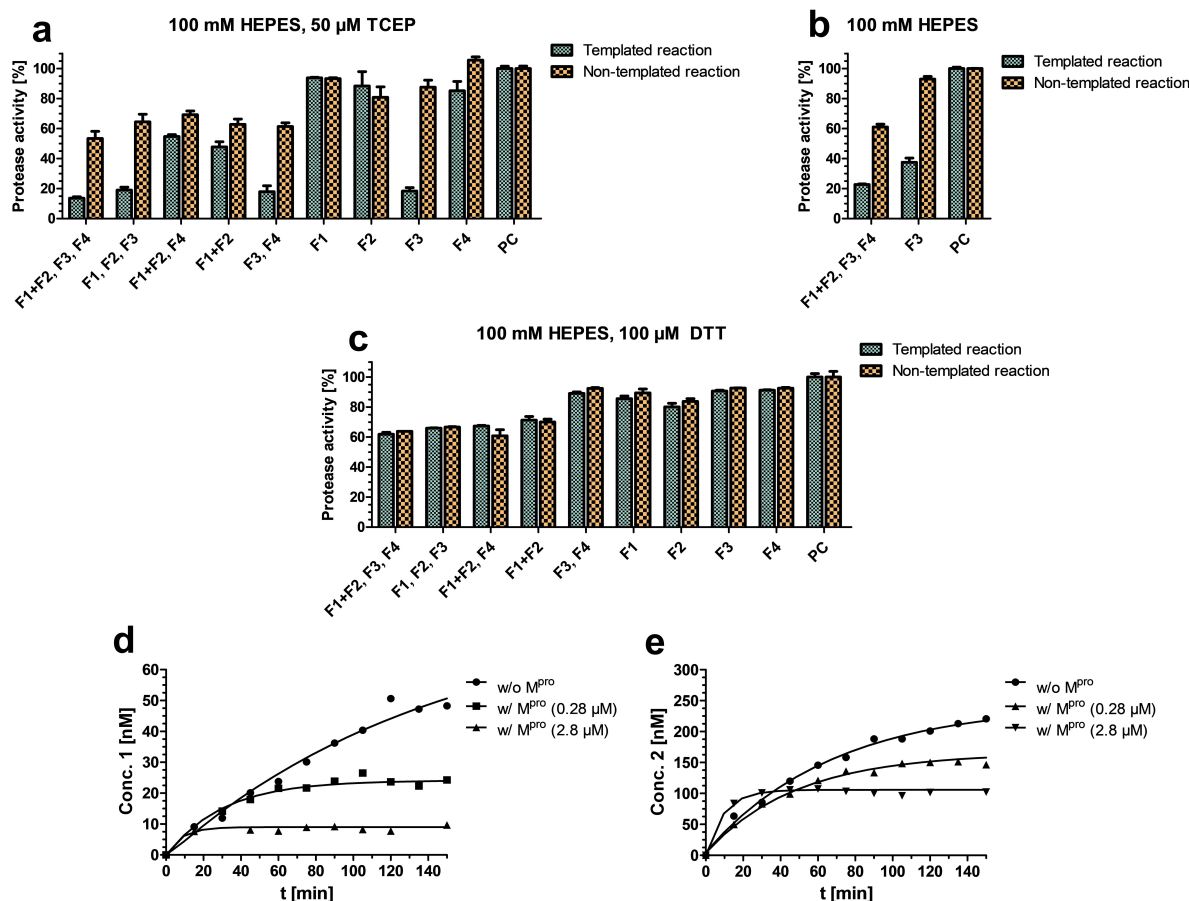


Figure 2. a–c. FRET-based inhibitor screening of fragments and fragment combinations (final concentrations after addition of substrate of F1 and F2: 0.8 mM, F3 and F4: 1.6 mM) after 2 h incubation at 20 °C with or without the M^{Pro} of SARS-CoV-2 at pH 8. a. HEPES-TCEP buffer (100 mM and 50 μ M, respectively). b. HEPES buffer (100 mM, without reducing agent). c. HEPES-DTT buffer (100 mM and 100 μ M, respectively). d–e. Quantitative monitoring of the Ugi 4CR and 3CR with or without SARS-CoV-2 M^{Pro} in HEPES-TCEP buffer (100 mM and 50 μ M, respectively) with HPLC-QTOF-MS for 150 min (F1 and F2: 1.5 mM, F3 and F4: 3.0 mM during incubation). The concentrations of 1 and 2 were plotted against the time and fitted with an exponential saturation function $c(t) = c_0 + (c_{\max} - c_0)(1 - e^{-kt})$. (For more details see Table 1 or Supporting Information); PC: positive control.

lower pH could be a better solubility of the employed fragments, accelerated imine formation or isonitrile addition to the imine. Differences in product formation between MOPS or HEPES buffer were negligible. In addition to Ugi products 1 and 2, traces of an amidine by-product 3 were found, formed from amine F2 and isocyanide F3, especially at lower pH values (Figure 1c).^[14] Several reaction pathways of carboxylic acids and isocyanides were reported in the literature,^[15] however, products of F3 with the acid F4 were not detected in our experiments. Only traces of the Passerini product 4 were detected at all tested pH values.^[16] In conclusion, HEPES buffers at pH 7 and pH 8, respectively, were selected for the investigation of the protein-templated reaction, in order to reduce the non-templated Ugi background reaction and formation of by-product 3. As a reducing agent is typically required to maintain the activity of SARS-CoV-2 main protease and to protect the active cysteine from oxidation,^[17] tolerance of the Ugi reaction for the reducing agents dithiothreitol (DTT) and tris(2-carboxyethyl) phosphine (TCEP) was investigated (Figure 1e). Addition of 50 mM DTT to 50 mM of each fragment F1–F4 in HEPES buffer pH 8 reduced the amount of the Ugi 4C

product 1 to about 20% of the control reaction without DTT as determined by HPLC-MS. At a DTT concentration of 5 mM, only a modest reduction of the conversion to 1 to about 80% was observed. In contrast, Ugi reactions in the presence of 5 or 50 mM TCEP showed no reduction of product formation.

Ugi reactions in presence of SARS CoV-2 main protease

To investigate protein-templated Ugi reaction, fragments F1, F2, F3, and F4 were incubated at different concentrations with SARS-CoV-2 M^{Pro} in HEPES buffer at pH 7 and pH 8 for 2 h alone and in all possible combinations of two, three or four fragments (Figure 2a–c). Either TCEP (50 μ M) or DTT (100 μ M) or no reducing agent was added. For the non-templated control experiments, every fragment and every fragment combination was incubated under identical conditions without protein, which was added after the 2 h incubation time. Subsequently, the activity of the protease was determined by addition of the fluorogenic substrate to the protein-templated reactions and the non-templated controls. No significant differences were

observed between the experiments conducted at pH 7 and 8, so that we employed pH 8 for all subsequent studies. Fragments **F1** and **F2** showed no significant inhibition of the protease at 0.8 mM, fragments **F3** and **F4** at 1.6 mM. Therefore, all templation experiments were conducted at these fragment concentrations. In the experiments with TCEP as reducing agent, all microtiter plate wells containing protein ("templated reactions") during the incubation showed stronger inhibition of the protease (up to >80%) than the non-templated controls (Figure 2a). Strongest inhibition was observed for the combination of all four fragments (**F1–F4**), the three-fragment combination **F1, F2, F3**, the two-fragment combination **F3, F4** and single fragment **F3** displayed similarly high inhibition in case of the templated reaction and less inhibition in the non-templated controls (Figure 2a). In comparison, incubation of fragments with protease in DTT-containing buffer did not result in higher inhibition in the protein-templated reactions (Figure 2c). While the reaction of four fragments **F1–F4** might lead to Ugi 4C product **1**, the observed inhibition in the three-fragment case (**F1, F2, F3**) might result from the formation of the Ugi 3CR product **2**. The combination of aldehyde **F1** and amine **F2** showed also enhanced inhibition (about 50%) in the templated case. As both fragments alone were almost inactive at the tested concentration, imine formation was suspected as the source of this inhibition and indeed in a solution of fragments **F1** and **F2** in DMSO an aldehyde-amine-imine equilibrium of 1:1:2 was observed by NMR spectroscopy, which of course might change in buffer at pH 8 (Supplementary Figure 3).^[18]

Isocyanide **F3** inhibited SARS-CoV-2 main protease after 2 h incubation in the presence of TCEP, but not with DTT, an observation demanding further investigation. Protease without freshly added reducing agents was inhibited by incubation with isocyanide as well, suggesting a direct interaction of the protein with the isocyanide (Figure 2b).^[17] Incubation of isocyanide **F3** with TCEP in buffer did not show a reaction product in HPLC-MS, whereas the reaction of **F3** with DTT (both at 1 M) in HEPES buffer (100 mM, pH 8) at room temperature overnight yielded two novel peaks in the HPLC, one with a mass corresponding to the addition product of DTT and **F3**, methanimidothioate **5** ($MH^+ = 286$ m/z),^[19] and the second one corresponding to the hydrolysis product of **F3**, formamide **6** ($MH^+ = 150$ m/z) (Supplementary Figure 4). Isolation of **5** was conducted by MPLC (Supplementary Figure 4, middle), and an NMR spectrum of the evaporated product fractions contained a mixture of formamide **6** together with the cyclic oxidation product of DTT (Supplementary Figure 4 bottom, Supplementary Figure S5). Similar interference of DTT as a competing nucleophile in fragment ligation assays has been reported recently and was resolved by replacement with TCEP as reducing agent.^[20] The observed reactivity of isocyanide **F3** with the thiol DTT might explain the observed time-dependent inhibition of the protease through a reaction with the active-site thiol.

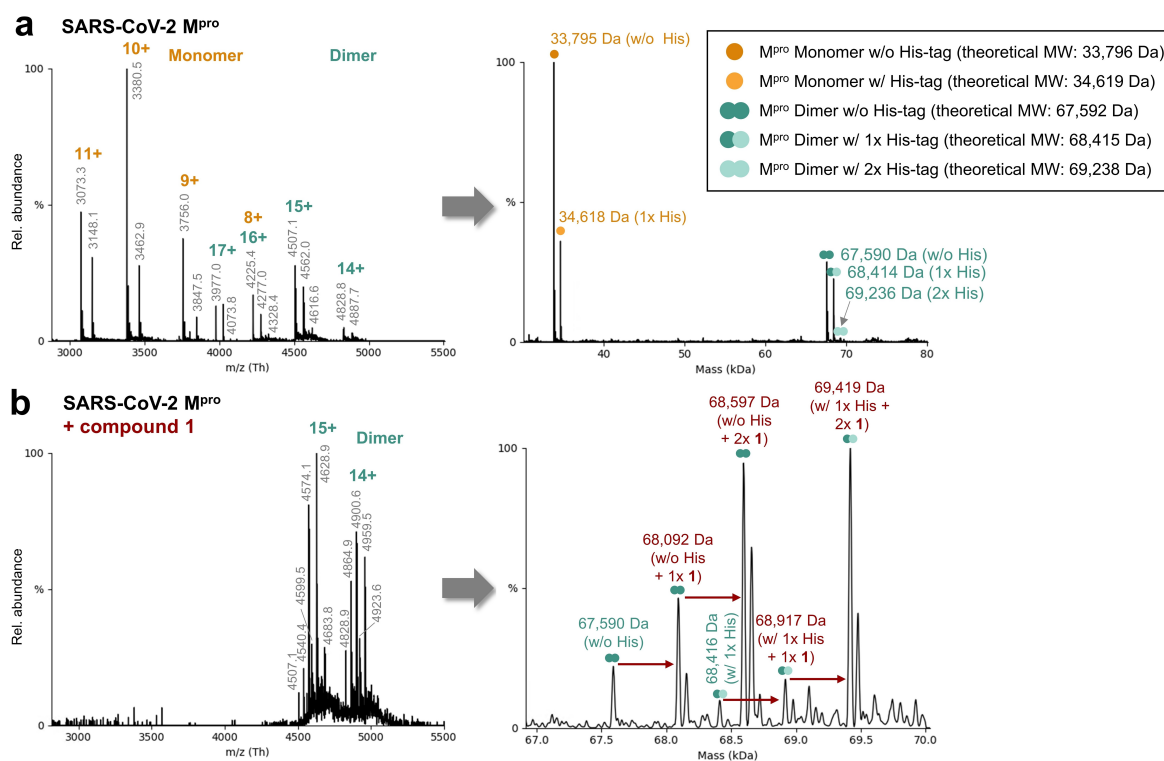


Figure 3. Characterization of Ugi product **1** binding to SARS-CoV-2 Mpro with native MS at pH 8. **a.** Raw spectrum of partially His-tagged SARS-CoV-2 Mpro (19 μ M) in the presence of 0.5% DMSO measured under native conditions (left) and corresponding deconvoluted spectrum (right). **b.** Raw spectrum of partial His-tagged SARS-CoV-2 Mpro (19 μ M) in the presence of 0.5% DMSO and compound **1** (38 μ M) measured under native conditions (left) and corresponding deconvoluted spectrum (right). Mass shifts induced by compound binding (theoretical MW: 502.2 Da) are indicated by red arrows.

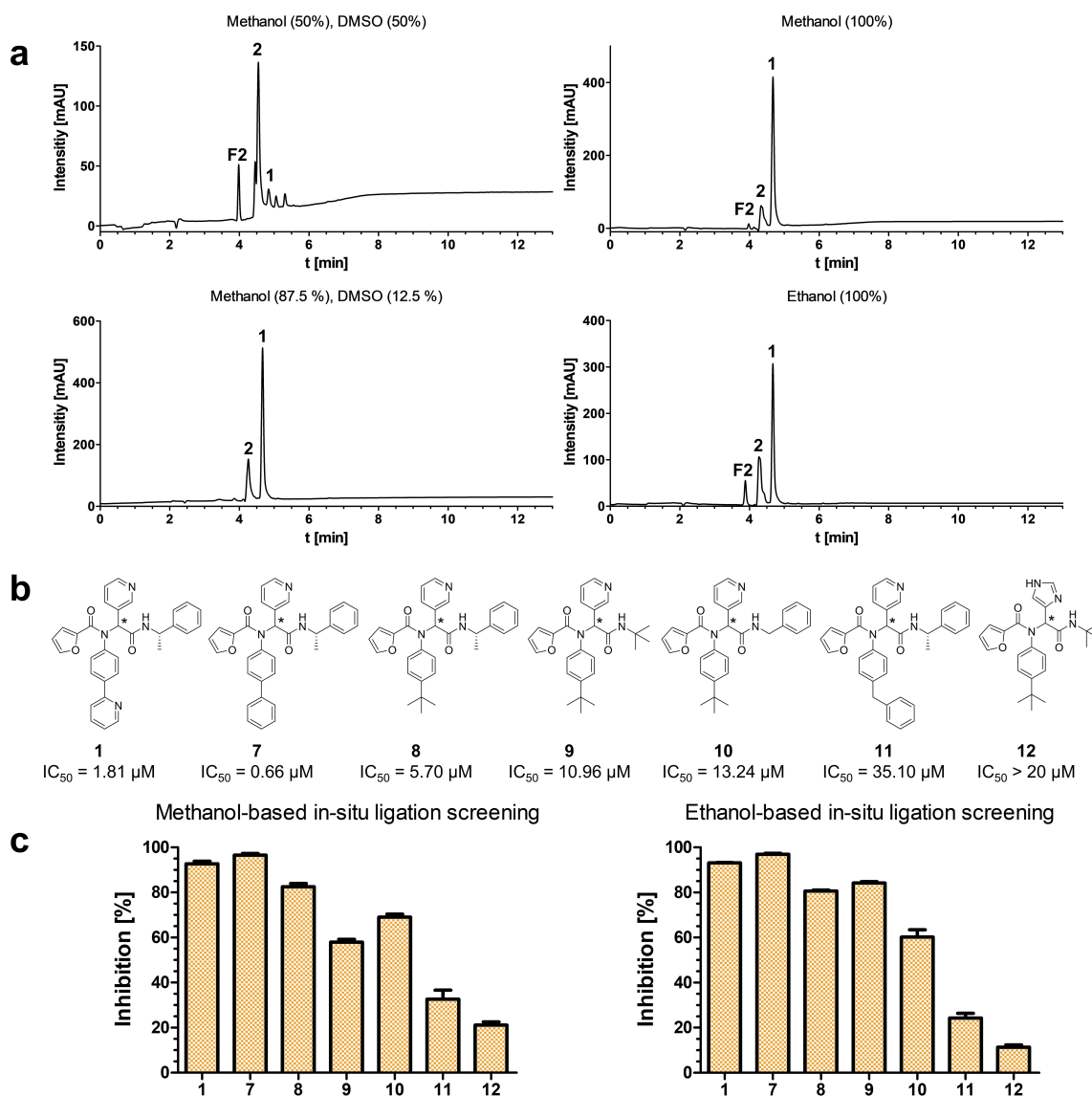


Figure 4. In-situ ligation screening of fragments forming Ugi-4CR products with M^{pro} of SARS-CoV-2. **a.** Monitoring of the in-situ reaction of fragments F1–F4 to compound 1 and 2 after 24 h at room temperature in various solvents. **b.** Inhibitors and their IC_{50} values.^[8b] **c.** Screening of the in-situ products 1 and 7–12 against the SARS-CoV-2 M^{pro} . Reactions were performed in methanol and ethanol at room temperature over 24 h and diluted with DMSO to result in a concentration of $10 \mu\text{M}$ of Ugi 4C product under the assumption of full conversion.

Quantitative analysis of Ugi product formation with and without SARS-CoV-2 M^{pro}

Next, formation of Ugi products 1 and 2 was monitored over time in the presence and absence of SARS-CoV-2 M^{pro} . Stock solutions of F1 and F2, F3 and F4 in DMSO were added to 100 mM HEPES buffer with $50 \mu\text{M}$ TCEP and incubated with and without protein for 150 min. Fragment concentrations were the same as in the protein templation experiments above before addition of substrate solution (F1 and F2: 1.5 mM , F3 and F4: 3.0 mM). Samples were analyzed quantitatively using HPLC-QTOF-MS. Concentrations of products 1 and 2 were determined from the integration of extracted ion signals using calibration curves, which were recorded from solutions of the analytes in the same buffer. Product concentrations were plotted over time

and fitted to an exponential saturation function $c(t) = c_0 + (c_{\text{max}} - c_0)(1 - e^{-kt})$ (Figure 2d–e, Table 1). Without protein (non-templated reaction), formation of products 1 and 2 followed saturation kinetics with half reaction times of 100 and 47 min, respectively, yielding maximal concentrations of 79 and 244 nM. Incubation with SARS-CoV-2 M^{pro} , to enable a templated reaction, decreased product formation to 24 and 165 nM, respectively, with $0.28 \mu\text{M}$ of protein, and to 9 and 106 nM with $2.8 \mu\text{M}$ protein. While higher protein concentration reduced product formation, the saturation rates increased in presence of the protein, suggesting a direct interference of the protease with the Ugi reaction. These results differed from those of protein-templated reactions, in which the acceleration of product formation and increase of product concentration were observed.^[2c,d,3] Similar observations of protein interference

Table 1. Quantitative determination of the product formation of compound 1 and 2 under the influence of SARS-CoV-2 M^{Pro} after 24 h. Experiments were conducted with the direct addition of the single fragments (F1, F2, F3, F4) and a preincubated stock solution of F1 and F2 (F1 + F2, F3, F4). Fitting of the determined concentrations against the time with the saturation function $c(t) = c_0 + (c_{\max} - c_0)(1 - e^{-Kt})$ resulted in the following values for the experiment with the preincubated mixture F1 + F2. (For raw data see Supplementary Table 1)

		F1 + F2, ^[a] F3, F4			$t_{1/2}$ [min]
		C_{24h} [nM]	C_{\max} [nM]	Saturation rate k [min^{-1}]	
Cpd. 1	w/o M ^{Pro}	79	79	0.007	100
	M ^{Pro} (0.28 μM)	22	24	0.033	21
	M ^{Pro} (2.8 μM)	13	9	0.118	6
Cpd. 2	w/o M ^{Pro}	244	244	0.015	47
	M ^{Pro} (0.28 μM)	178	165	0.021	34
	M ^{Pro} (2.8 μM)	128	106	0.105	7

[a] Preincubation of F1 and F2 for 19.5 h at 20 °C.

have been reported in case of the Groebke–Blackburn–Bienaymé reaction earlier.^[9] Several reasons might explain the absence of protein-templated Ugi reactions in our experiments. Fragment concentrations required for efficient product formation were higher than in the reported successful examples of protein-templated reactions. Especially the rate-determining step within the Ugi reaction sequence, the addition of isonitrile to the imine requires high concentration to reach an acceptable turnover. These high fragment concentrations resulted in interactions of the imine (F1 + F2) or isocyanide F3 fragments with the protein leading to the observed inhibition of the protease and decreased the yield of the Ugi reaction.

Native MS of SARS-CoV-2 main protease with Ugi product 1

Protein-templated Ugi reactions of fragments F1–F4 were additionally investigated by native mass spectrometry of SARS-CoV-2 main protease, a method which is capable of detecting protein-ligand complexes formed due to both covalent and non-covalent interactions. For native MS, the buffer of SARS-CoV-2 M^{Pro} was exchanged to 200 mM ammonium acetate pH 8 and protein mass spectra were recorded with and without the addition of the resynthesized Ugi product 1. The mass spectrum of M^{Pro} without inhibitor revealed two main charge state distributions corresponding to a mixture of the monomeric and dimeric proteins with the His-tag partially cleaved (Figure 3a). Dominant signals were measured at 33,795 Da (monomer) and 67,590 Da (dimer), respectively, and corresponded to the protein without the His-tag (theoretical MW: 33,796 Da for the monomer and 67,592 Da for the dimer). After incubation with Ugi product 1, the monomeric protein signals disappeared, while the dimer signals dominated the spectrum (Figure 3b). These findings indicate the ligand-induced dimerization of the SARS-CoV-2 M^{Pro} and the stabilization of the dimeric form, which is demonstrated here for the first time by native MS.

Dimerization of SARS-CoV-2 M^{Pro} has been reported before in protein crystallization and has been confirmed for SARS-CoV-1 M^{Pro} by using analytical ultracentrifugation.^[21] Accordingly, in our experiments with the addition of Ugi product 1 (theoretical MW: 502.2 Da), additional signals became dominant in the spectrum, which were in agreement with the binding of one and two inhibitor molecules to the protein dimer (Figure 3b). The presence or absence of the His-tag showed no influence on the interaction. Using source-induced dissociation (SID) the inhibitor was dissociated from the dimer at higher collision energies in the gas-phase, showing the non-covalent nature of the interaction (not shown). In summary, native MS confirmed the specific non-covalent binding of two molecules of Ugi product 1 to the protein dimer of SARS-CoV-2 M^{Pro} in a 2:1 stoichiometry.

Next, the protein-templated Ugi reaction of the M^{Pro} was investigated by native MS. For a protein-templated formation of Ugi 4 CR products, the fragments were hypothesized to bind to the protease and might also lead to a shift in the monomer-dimer equilibrium. Therefore, M^{Pro} (18 μM) was incubated with 500 μM of fragments F1–F4 for 2 h in ammonium acetate buffer and diluted with buffer prior to the native MS measurements. The resulting spectra showed additional mass peaks corresponding to the 4CR Ugi product of F1–F3 and acetic acid, proving again the occurrence of the Ugi reaction even at high excess of ammonium acetate buffer and at lower fragment concentrations (Supplementary Figure S6). The formation of Ugi product 1, however, was not observed, most likely due to the high concentration of acetate in the buffer which participated instead of F4 in the Ugi reaction. Native protein MS showed no additional mass signals due to ligand binding and no increased signals of the protein dimer, confirming that no ligand had shifted the monomer-dimer equilibrium.

In-situ ligation screening for inhibitors of SARS-CoV-2 M^{Pro} using the Ugi 4C reaction

Having demonstrated the fast and efficient conversion of reactive fragments to Ugi 4CR product 1 and the interference of the protein target with templated reactions, in-situ ligation screening of Ugi products as SARS-CoV-2 M^{Pro} inhibitors was investigated as a potential alternative method.^[22] The aim was to identify reaction conditions operated in microtiter plates which enabled maximal conversion to Ugi 4C products and direct testing in the enzyme assay without the need for work-up or purification. Various solvents were investigated for the in-situ preparation of a library of Ugi products using compound 1 as a reference. Neat DMSO, the standard solvent for screening libraries used in automated bioassays, yielded no Ugi 4CR product 1. Thus, neat methanol and ethanol were investigated in combinations with DMSO. For the purpose, stock solutions of the four fragments F1–F4 were prepared in DMSO, methanol, and ethanol (500 mM or 1 M) and reacted in mixtures with fragment concentrations of 125 mM at room temperature. After 24 h, the crude mixtures were analyzed by HPLC-MS for product formation. The 1:1 mixture of methanol and DMSO furnished

the 3CR product **2** as the major product (integration 100%) and less than 20% of the 4C product **1** was formed (Figure 4a). In contrast, neat methanol accelerated the Ugi 4CR and showed almost complete conversion to product **1** suppressing conversion to the 3CR product **2** to less than 15%. Interestingly, already 12.5% of DMSO enhanced the 3CR to more than 20%. In ethanol, being less volatile and having a higher viscosity than methanol, the 4CR-product **1** was still the major product, however, approximately one third of the of 3CR product **2** was formed.

Next, in-situ ligation screening of fragments forming a small collection of SARS-CoV-2 M^{Pro} inhibitors^[8b] was conducted. Stock solutions of 10 fragments (500 mM) in methanol and ethanol were prepared, furnishing in Ugi products (Figure 4b). After 20 h, the crude mixtures were analyzed regarding their conversion rates to the Ugi 4CR product. In all experiments and in both solvents, the Ugi 4CR products were formed; the conversion and purity of products were quantified by HPLC-MS using integration of the UV signals at 254 nm (Supplementary Figures S7 and S8). All crude reaction mixtures were diluted with DMSO to the concentration of 10 μM Ugi product, under the assumption of full conversion, and tested in the described fluorescence-based assay for their inhibition of SARS-CoV-2 M^{Pro} (Figure 4c). This dilution protocol resulted in methanol and ethanol concentrations in the assays below 0.01% (v/v), which did not affect the enzyme activity as demonstrated by control samples. All inhibitors with IC₅₀ values around or below 10 μM showed inhibition >50% in the assay, indicating a strict correlation between the results of in-situ ligation screening of fragments and the testing of isolated Ugi 4CR products. The highest inhibition of over 95% was detected for the reaction mixture yielding **7** in both solvents, corresponding to the lowest IC₅₀ value of all investigated compounds (IC₅₀ = 0.66 μM). Only Ugi products **11** and **12** with IC₅₀ values of >20 μM displayed <40% inhibition in the in-situ ligation assay, identifying these negative control compounds as inactive. In summary, at least for this small selection of reactions and for this specific protein target, in-situ ligation screening of fragments forming Ugi products appears to be a fast and efficient method for the synthesis and testing of compounds with considerably complexity, which are capable to occupy up to four adjacent binding pockets with one small molecule. The method has been established here for the identification of SARS-CoV-2 protease inhibitors, suggesting that this concept should be applicable to other protein targets as well. For the Ugi reaction, in-situ ligation screening of fragments appears to be superior to the protein-templated formation of inhibitors.

Conclusions

In summary, we have investigated protein-templated Ugi four-component reactions (4CR) with SARS-CoV-2 main protease and their potential and limitations for the efficient screening for protease inhibitors. We have demonstrated that Ugi 4CR proceeded efficiently in aqueous protein buffers over a broad pH range using TCEP but not DTT as a reductant and in alcohols

such as methanol and ethanol. Starting from fragments **F1–F4** inhibition of the enzyme SARS-CoV-2 M^{Pro} was observed in the enzyme activity assays and formation of the potent inhibitor **1** in presence of the protein was confirmed by HPLC-QTOF-MS analysis. Fragment concentrations required to observe inhibition of the protein, however, were much higher (0.8–1.6 mM) than those typically employed in fragment ligation screening (max. 0.1–0.2 mM), supposedly as the rate-determining step in the Ugi reactions, the isocyanide addition to the imine, was significantly slower as in those reactions studied earlier. At these concentrations, the protein, SARS-CoV-2 M^{Pro}, did not accelerate inhibitor formation as defined for protein-templated reactions. There are several observations which might explain the reduced turnover of the fragments in presence of the protein target. The isocyanide fragment and the imine fragment combination were found to inhibit the protease, possibly blocking the active site for conversion to the final Ugi product and resulting in the reduced SARS turnover of the protein-templated reaction. While product **1** fits into the active site as indicated by its inhibitory activity, the key intermediary imidate, which undergoes the Mumm rearrangement to the Ugi product,^[5,7] might not be able to bind to the protein target. Native MS studies confirmed the binding of the Ugi 4CR product **1** to SARS-CoV-2 M^{Pro}. Binding of the inhibitor shifted the protein equilibrium from the protein monomer to the protein dimer, resulting in the protein dimer with two inhibitor molecules bound as the dominant protein-ligand complex. Ugi 4CR were also observed under native MS conditions, however, not the inhibitor **1** was formed but the Ugi product with the buffer component acetic acid as the acidic component. The suspected addition product between the active site cysteine and the isocyanide could not be detected in native MS.

Considering the limitations of protein-templated Ugi reactions, in-situ ligation screening of Ugi 4CR products with SARS-CoV-2 M^{Pro} was found to be a powerful alternative. Ugi products were formed in high purity when using methanol or ethanol for the in-situ reactions and could be screened in the SARS-CoV-2 main protease assay after dilution with DMSO. Enzyme inhibition recorded in this assay corresponded precisely with the reported IC₅₀ values for all tested Ugi products. Thus, for Ugi four-component reactions in-situ ligation screening is a viable and very efficient alternative to protein-templated reaction as a strategy to identify more potent, fragment-based inhibitors. We anticipate that this conclusion does apply not only for the main protease of SARS-CoV-2 as a target but to other proteases and target classes with binding sites constructed of several adjacent sub-pockets, which can be addressed by fragment ligation products.

Experimental Section

General methods

All chemicals, purchased from Sigma-Aldrich (Steinheim, Germany), abcr GmbH (Karlsruhe, Germany), Carl Roth GmbH & Co. KG (Karlsruhe, Germany), and TCI Deutschland GmbH (Eschborn, Germany), were used without further purifications.

Reaction controls were conducted with an Agilent 1100 LC–MS system. A Biotage Isolera One (MPLC) or an Agilent 1260 Infinity Binary LC (HPLC) were used for the purification of the synthesized compounds. If not specified otherwise, chromatography (silica or RP-18 HPLC), high-resolution mass spectrometry, and fully assigned ^1H - and ^{13}C -NMR spectra confirmed the identity and purity (> 95%) of the synthesized compounds. ^1H and ^{13}C NMR spectra were recorded with Jeol ECZ600 or AVANCE700 spectrometers.

Detailed explanations of additional methods, protocols, and chemical syntheses are reported in the Supporting Information.

FRET-based enzyme assay for the detection of a protein templated Ugi reaction

The assays were measured with a TECAN Infinite M1000 microplate reader. The stock solution of SARS-CoV-2 main protease was diluted with buffer (100 μM DTT or 50 μM TCEP, 100 mM HEPES, pH 8), resulting in 1 μM protein ($M^{\text{pro}}_{\text{a}}$). The four fragments F1–F4 were dissolved in DMSO (100 mM). Fragment F1 and F2 were mixed prior to the experiment (1:1). In 384 well plates (Corning 3766, black with clear flat bottom, non-binding surface), buffer (20 μl) and protease solution (10 μl) were added first, followed by the addition of the fragment stock solutions F1 + F2, F3, and F4 (1 μl each, 50 mM or 100 mM stock solutions in DMSO). Controls were prepared with buffer (10 μl) instead of protease for the non-templated reactions. The well plate was shaken for 30 s (1250 rpm) and centrifuged (1000 rpm, 10 s). Afterwards, the plate was additionally shaken for 2 h at 20 $^{\circ}\text{C}$. After the incubation, buffer (10 μl) was added to the wells with protease, and protease solution (10 μl) was added to the non-templated reaction controls. The plate was shaken for 30 s (1250 rpm) and centrifuged (1000 rpm, 10 s). The FRET substrate solution (20 μl of a 10 μM solution of Dabcyl-KTSAVLQ/SGFRKM-E(Edans)-amide (Biosyntan GmbH, Berlin, Germany) in buffer and 0.5% DMSO) was added, and the plate was shaken and centrifuged again. Positive controls were recorded with DMSO instead of inhibitor solution for both, the templated reaction wells and the non-templated reaction wells. Additionally, negative controls were prepared with buffer instead of protease solution. Fluorescence increase [RFU/min] was measured over 15 min and normalized to the corresponding positive controls. The percentage of inhibition was calculated and illustrated in Graphpad Prism.

Monitoring of the Ugi product formation with HPLC-QTOF-MS

Protease solution (40 μl , 9 μM or 0.9 μM , $M^{\text{pro}}_{\text{b}}$) was diluted with buffer (80 μl , 100 mM HEPES, 50 μM TCEP) and shaken for a few minutes at 20 $^{\circ}\text{C}$ to adjust to room temperature. Afterwards, stock solutions of the four fragments in DMSO (F1, F2: 2 μl , 100 mM, F3, F4: 4 μl , 100 mM) were added to result in total concentrations of 2.8 or 0.28 μM M^{pro} , 1.5 mM F1 and F2, and 3.0 mM F3 and F4. The resulting fragment concentrations were chosen accordingly to the concentrations during incubation of the FRET-based enzyme assays. For the investigation of the effect of a premixed imine stock solution, F1 (20 μl , 100 mM) and F2 (20 μl , 100 mM) were mixed and shaken for 19.5 h at 20 $^{\circ}\text{C}$. To the diluted protease solution (40 μl $M^{\text{pro}}_{\text{b}}$ (9 μM or 0.9 μM) and 80 μl buffer (100 mM HEPES; 50 μM TCEP)), the preincubated mixture F1 + F2 (4 μl , 50 mM), F3, and F4 (4 μl , 100 mM, respectively) were added. Controls without protease were prepared, using buffer (40 μl , 100 mM HEPES; 50 μM TCEP) instead of protease solution for both experiments. The six mixtures were shaken at 20 $^{\circ}\text{C}$ (1250 rpm) and samples were taken every 15 minutes for 150 min and after 24 h. Every sample was quenched with formic acid, diluted with acetonitrile (1:2), and analyzed by HPLC-QTOF-MS (Agilent 1290 Infinity II coupled with an Agilent 6550 iFunnel QToF), using an adapted version of the

previously reported instrument method.^[11] For quantification of the formed Ugi products, calibration curves were recorded by plotting the integrated signal intensities (AUC) of the extracted ion chromatograms of Ugi products 1 and 2 from dilution series of the Ugi products 1 and 2 in the range of 3.9–250 nM and 5.6–1000 nM, respectively, with the same amounts of HEPES-TCEP buffer (48%), DMSO (5%), formic acid (5%) and acetonitrile (42%) and were measured with the same method as for the templation experiments in duplicates (Supplementary Figure S9). Evaluation was conducted, using Masshunter QTOF-Quantification Software of Agilent and Graphpad Prism for fitting of the amount of product against the time to an exponential saturation function $c(t) = c_0 + (c_{\text{max}} - c_0)(1 - e^{-kt})$. HPLC parameters: injection volume: 1 μl , column: Zorbax Eclipse plus C18 RRHD (1.8 μM , 95 \AA , 2.1 \times 50 mm) from Agilent, mobile phase: water (A) and acetonitrile (B) with 0.1% formic acid, flow rate: 0.5 ml/min, gradient: 0–8 min from 95/5 (A/B) to 5/95 (A/B), 8–9 min 5/95 (A/B), 9–10 min from 5/95 (A/B) to 95/5 (A/B), 0–2 min waste. QTOF parameters: positive mode, gas temperature 200 $^{\circ}\text{C}$, gas flow 11 l/min, nebulizer 35 psig, sheath gas temperature 375 $^{\circ}\text{C}$, sheath gas flow 11 l/min, octopole RF peak 750, fragmentor 175 V, nozzle voltage 500 V, VCap 3500 V.

Native mass spectrometry with SARS-CoV-2 M^{pro}

The expression buffer of SARS-CoV-2 M^{pro} (42 μM , $M^{\text{pro}}_{\text{a}}$) was exchanged using a Vivaspin 500 cut-off filter (MWCO 10,000) for an ammonium acetate buffer (200 mM, adjusted to pH 8 with NH_4OH). To avoid precipitation during buffer exchange due to high protein concentrations, the protease was diluted 1:2 prior to centrifugation with the ammonium acetate buffer and then centrifuged at 12,000 $\times g$ at 4 $^{\circ}\text{C}$ for 3 minutes. This procedure was repeated 16 times in order to ensure quantitative buffer exchange. The protein was stored in aliquots at -80°C (final concentration: 19 μM).

For native MS measurements, a DMSO stock solution of Ugi product 1 (50 mM) was diluted with 200 mM ammonium acetate buffer. The diluted stock solution was mixed with the M^{pro} to result in final concentrations of 18 μM M^{pro} and 38 μM Ugi product 1 with 0.5% DMSO. As a control, 18 μM M^{pro} with 0.5% DMSO was prepared. In addition, stock solutions of the four fragments F1–F4 (400 mM) were prepared in DMSO and mixed to result in concentrations of 100 mM each. After further dilution with ammonium acetate, the fragment mix was added to the SARS-CoV-2 M^{pro} and incubated for 2 h at room temperature (M^{pro} : 18 μM , F1–F4: 500 μM , 0.5% DMSO). Before measurement, the sample was diluted 1:5 to avoid ion suppression due to the high fragment concentrations, resulting in 4 μM M^{pro} and 100 μM F1–F4.

The native MS measurements were performed on a Q Exactive HF mass spectrometer using direct injection with an offline nanoESI source head on the NanoFlex ion source (Thermo Scientific). The intact protein mode was activated, and the trapping gas pressure was set to 0.2 (available with Biopharma option). All spectra were recorded for at least 30 s in the profile mode with positive polarity using the following settings: scan range 1,500 to 6,000 m/z, resolution 15,000, microscans 5, AGC target 3e6, maximum inject time 200 ms, spray voltage 2.2 kV, capillary temperature 175 $^{\circ}\text{C}$, S-lens RF level 200, source-induced dissociation (SID) 75 eV. For fragment detection the lower limit of the scan range was set to 100 m/z. The software tool UniDec was used for data processing and deconvolution.^[23] First, an averaged spectrum was generated from each measurement followed by spectral deconvolution using the default settings with following modifications: charge range 5–20, Mass range 30–70 kDa, sample mass every 1 Da.

In-situ screening for inhibitors against the M^{pro} of SARS-CoV-2 with the Ugi-4CR

Stock solutions (500 μ M) in methanol and ethanol were prepared for the following fragments: 3-pyridinecarboxaldehyde, 4-imidazolecarboxaldehyde, 4-aminobiphenyl, 4-(2-pyridyl)-aniline, 4-tert-butylaniline, 4-benzylaniline, (S)-(–)- α -methylbenzyl isocyanide, tert-butyl isocyanide, benzyl isocyanide, 2-furoic acid. Solubility problems occurred for 4-aminobiphenyl and 4-(pyridine-2-yl)-aniline in methanol.

Four-fragment combinations were mixed accordingly in equimolar volumes and reacted over night for 24 h at room temperature to obtain the seven Ugi products **1** and **7–12**. Samples (1 μ l) were taken from each reaction and diluted with water-acetonitrile mixture (399 μ l, 1/1) and analyzed on an Agilent 1100 HPLC-MS system with an UV detector at 245 nm using the previously published instrument method.^[11] Evaluation of the chromatograms were performed with Agilent ChemStation and GraphPad Prism. HPLC parameters: injection volume: 3 μ l, column: Luna C18(2) (3 μ m, 100 Å, 100 \times 4.6 mm) from phenomenex, mobile phase: water (A) and acetonitrile (B) with 0.1% formic acid, flow rate: 1 ml/min, gradient: 0–5.5 min from 95/5 (A/B) to 1/99 (A/B), 5.5–10 min 1/99 (A/B), 10–12 min from 1/99 (A/B) to 95/5 (A/B).

For the in-situ screening, the crude mixtures were diluted with DMSO to result in product concentrations of 10 μ M with the assumption of complete conversion (0.01% methanol and ethanol content) and were screened in the fluorescence-based protease assays described above (see “Activity screening with SARS-CoV-2 M^{pro} and determination of IC₅₀ values”). Positive and negative controls with the same methanol or ethanol content were prepared.

Supporting Information^[25]

Supplementary Table 1, Supplementary Figures 1 to 15, and Supplementary Methods are provided in the Supporting Information.

Acknowledgements

The work was funded by the Deutsche Forschungsgemeinschaft (DFG, German Research Foundation) – Project-ID 387284271 – SFB 1349 (Project A3) and China Scholarship Council (CSC). For mass spectrometry, the authors acknowledge the assistance of the Core Facility BioSupraMol supported by the DFG. The authors thank C. Weise for critical reading. Open Access funding enabled and organized by Projekt DEAL.

Conflict of Interests

The authors declare no conflict of interest.

Data Availability Statement

The data that support the findings of this study are available in the supplementary material of this article.

Keywords: antiviral agents · multicomponent reactions · protein-templated reactions · SARS-CoV-2 main protease · Ugi reaction

- [1] a) For a review: M. Jaegle, E. L. Wong, C. Tauber, E. Nawrotzky, C. Arkona, J. Rademann, *Angew. Chem. Int. Ed.* **2017**, *56*, 7358–7378; b) For a seminal work on protein-templated reactions, see: W. G. Lewis, L. G. Green, F. Grynszpan, Z. Radic, P. R. Carlier, P. Taylor, M. G. Finn, K. B. Sharpless, *Angew. Chem. Int. Ed.* **2002**, *41*, 1053–1057.
- [2] a) M. F. Schmidt, A. Isidro-Llobet, M. Lisurek, A. El-Dahshan, J. Tan, R. Hilgenfeld, J. Rademann, *Angew. Chem. Int. Ed.* **2008**, *47*, 3275–3278; b) M. Schmidt, A. El-Dahshan, S. Keller, J. Rademann, *Angew. Chem.* **2009**, *48*, 6346–6349; c) E. Burda, J. Rademann, *Nat. Commun.* **2014**, *5*, 5170; d) D. Becker, Z. Kaczmarek, C. Arkona, R. Schulz, C. Tauber, G. Wolber, R. Hilgenfeld, M. Coll, J. Rademann, *Nat. Commun.* **2016**, *7*, 12761; e) M. Jaegle, T. Steinmetzer, J. Rademann, *Angew. Chem. Int. Ed.* **2017**, *56*, 3718–3722; f) C. Tauber, R. Wamser, C. Arkona, M. Tügend, U. B. A. Aziz, S. Pach, R. Schulz, D. Jochmans, G. Wolber, J. Neyts, J. Rademann, *Angew. Chem. Int. Ed.* **2021**, *60*, 13294–13301.
- [3] E. L. Wong, E. Nawrotzky, C. Arkona, B. G. Kim, S. Belygin, X. Wang, S. Wagner, M. Lisurek, D. Carstensen, J. Rademann, *Nat. Commun.* **2019**, *10*, 66.
- [4] a) M. Passerini, L. Simone, *Gazz. Chim. Ital.* **1921**, *51*, 126–129; b) M. Passerini, *Gazz. Chim. Ital.* **1921**, *51*, 181–189.
- [5] a) I. Ugi, R. Meyr, U. Fetzer, C. Steinbrückner, *Angew. Chem.* **1959**, *71*, 373–388; b) I. Ugi, C. Steinbrückner, *Angew. Chem.* **1960**, *72*, 267–268.
- [6] a) A. Dömling, I. Ugi, *Angew. Chem. Int. Ed.* **2000**, *39*, 3168–3210; b) A. Dömling, *Chem. Rev.* **2006**, *106*, 17–89; c) A. Barthelon, L. El Kaïm, M. A. Gizolme, L. Grimaud, *Eur. J. Org. Chem.* **2008**, *2008*, 5974–5987; d) M. A. Fouad, H. Abdel-Hamid, M. S. Ayoub, *RSC Adv.* **2020**, *10*, 42644–42681; e) N. P. Tripolitsiotis, M. Thomaidi, C. G. Neochoritis, *Eur. J. Org. Chem.* **2020**, 6525–6554; f) L. Banfi, A. Basso, C. Lambruschini, L. Moni, R. Riva, *Chem. Sci.* **2021**, *12*, 15445–15472; g) Y. Wahby, H. Abdel-Hamid, M. S. Ayoub, *New J. Chem.* **2022**, *46*, 1445–1468; h) S. E. Hooshmand, W. Zhang, *Molecules* **2023**, *28*, 1642.
- [7] N. Chéron, R. Ramozzi, L. El Kaïm, L. Grimaud, P. Fleurat-Lessard, *J. Org. Chem.* **2012**, *77*, 1361–1366.
- [8] a) J. Jacobs, V. Grum-Tokars, Y. Zhou, M. Turlington, S. A. Saldanha, P. Chase, A. Eggler, E. S. Dawson, Y. M. Baez-Santos, S. Tomar, A. M. Mielech, S. C. Baker, C. W. Lindsley, P. Hodder, A. Mesecar, S. R. Stauffer, *J. Med. Chem.* **2013**, *56*, 534–546; b) N. Kitamura, M. D. Sacco, C. Ma, Y. Hu, J. A. Townsend, X. Meng, F. Zhang, X. Zhang, M. Ba, T. Szeto, A. Kukuljac, M. T. Marty, D. Schultz, S. Cherry, Y. Xiang, Y. Chen, J. Wang, *J. Med. Chem.* **2022**, *65*, 2848–2865; c) C. Ma, Z. Xia, M. D. Sacco, Y. Hu, J. A. Townsend, X. Meng, J. Choza, H. Tan, J. Jang, M. V. Gongora, X. Zhang, F. Zhang, Y. Xiang, M. T. Marty, Y. Chen, J. Wang, *J. Am. Chem. Soc.* **2021**, *143*, 20697–20709; d) J. K. Stille, J. Tjuttrins, G. Wang, F. A. Venegas, C. Hennecker, A. M. Rueda, I. Sharon, N. Blaine, C. E. Miron, S. Pinus, A. Labarre, J. Plescia, M. Burai Patrascu, X. Zhang, A. S. Wahba, D. Vlaho, M. J. Huot, T. M. Schmeing, A. K. Mittermaier, N. Moitessier, *Eur. J. Med. Chem.* **2022**, *229*, 114046; e) K. Rossen, P. J. Pye, L. M. DiMichele, R. P. Volante, P. J. Reider, *Tetrahedron Lett.* **1998**, *39*, 6823–6826; f) I. Ugi, R. Meyr, *Chem. Ber.* **1961**, *94*, 2229–2233; g) J. U. Nef, *Justus Liebig's Ann. Chem.* **1892**, *270*, 267–335; h) L. Banfi, A. Basso, G. Guanti, R. Riva, in *Multicomponent Reactions* (Eds.: J. Zhu, H. Bienaymé), Wiley-VCH, Weinheim, **2005**, pp. 1–32; i) C. Faggi, M. García-Valverde, S. Marcaccini, G. Menchi, *Org. Lett.* **2010**, *12*, 788–791; j) N. Chéron, L. El Kaïm, L. Grimaud, P. Fleurat-Lessard, *J. Phys. Chem. A* **2011**, *115*, 10106–10112; k) H. D. Preschel, R. T. Otte, Y. Zhuo, R. E. Ruscoe, A. J. Burke, R. Kellerhals, B. Horst, S. Hennig, E. Janssen, A. P. Green, N. J. Turner, E. Ruijter, *J. Org. Chem.* **2023**, *88*, 12565–12571.
- [9] R. Gladysz, J. Vrijdag, D. Van Rompaey, A.-M. Lambeir, K. Augustyns, H. De Winter, P. Van der Veken, *Chem. Eur. J.* **2019**, *25*, 12380–12393.
- [10] F. Mancini, M. Y. Unver, W. A. M. Elgaher, V. R. Jumde, A. Alhayek, P. Lukat, J. Herrmann, M. D. Witte, M. Köck, W. Blankenfeldt, R. Müller, A. K. H. Hirsch, *Chem. Eur. J.* **2020**, *26*, 14585–14593.
- [11] R. Wamser, S. Pach, C. Arkona, M. Baumgardt, U. B. A. Aziz, A. C. Hocke, G. Wolber, J. Rademann, *ChemMedChem* **2023**, *18*, e202200635.
- [12] S. C. Pan, B. List, *Angew. Chem. Int. Ed.* **2008**, *47*, 3622–3625.
- [13] a) J. Breidenbach, C. Lemke, D. T. Pillaiyar, L. Schäkel, G. A. Hamwi, M. Dieltz, R. Gedschold, N. Geiger, V. Lopez, S. Mirza, D. V. Namasivayam, D. A. C. Schiedel, K. Sylvester, D. D. Thimm, C. Vielmuth, L. P. Vu, M. Zylulina, P. D. J. Bodem, P. D. M. Gütschow, P. D. C. E. Müller, *Angew.*

- Chem. Int. Ed.* **2021**, *60*, 10423–10429; b) S. Legare, F. Heide, B. A. Bailey-Elkin, J. Stetefeld, *J. Biol. Chem.* **2022**, *298*, 101739; c) Q. Hu, Y. Xiong, G.-H. Zhu, Y.-N. Zhang, Y.-W. Zhang, P. Huang, G.-B. Ge, *MedComm* **2022**, *3*, e151.
- [14] a) T. L. Davis, W. E. Yelland, *J. Am. Chem. Soc.* **1937**, *59*, 1998–1999; b) T. Saegusa, Y. Ito, S. Kobayashi, K. Hirota, H. Yoshioka, *Bull. Chem. Soc. Jpn.* **1969**, *42*, 3310–3313; c) C. Cao, Y. Shi, A. L. Odom, *J. Am. Chem. Soc.* **2003**, *125*, 2880–2881; d) K. Ostrowska, A. Kolasa, in *Category 3, Compounds with Four and Three Carbon Heteroatom Bonds, Vol. 22* (Ed.: A. B. Charette), Georg Thieme Verlag KG, Stuttgart, **2005**; e) O. Ghashghaei, M. Revés, N. Kielland, R. Lavilla, *Eur. J. Org. Chem.* **2015**, *2015*, 4383–4388; f) E. S. Smirnova, J. M. Muñoz Molina, A. Johnson, N. A. G. Bandeira, C. Bo, A. M. Echavaren, *Angew. Chem. Int. Ed.* **2016**, *55*, 7487–7491.
- [15] a) A. Shaabani, E. Soleimani, A. H. Rezayan, *Tetrahedron Lett.* **2007**, *48*, 6137–6141; b) X. Li, S. J. Danishefsky, *J. Am. Chem. Soc.* **2008**, *130*, 5446–5448; c) Y. Rao, X. Li, S. J. Danishefsky, *J. Am. Chem. Soc.* **2009**, *131*, 12924–12926.
- [16] a) Y. Y. Lim, A. R. Stein, *Can. J. Chem.* **1971**, *49*, 2455–2459; b) J. Azuaje, A. Coelho, A. E. Maatougui, J. M. Blanco, E. Sotelo, *ACS Comb. Sci.* **2011**, *13*, 89–95.
- [17] J. McNulty, V. Krishnamoorthy, D. Amoroso, M. Moser, *Bioorg. Med. Chem. Lett.* **2015**, *25*, 4114–4117.
- [18] C. Godoy-Alcántar, A. K. Yatsimirsky, J. M. Lehn, *J. Phys. Org. Chem.* **2005**, *18*, 979–985.
- [19] a) T. Saegusa, S. Kobayashi, K. Hirota, Y. Okumura, Y. Ito, *Bull. Chem. Soc. Jpn.* **1968**, *41*, 1638–1642; b) T. Saegusa, S. Kobayashi, Y. Ito, *J. Org. Chem.* **1970**, *35*, 2118–2121; c) P. Mampuy, Y. Zhu, S. Sergeev, E. Ruijter, R. V. A. Orru, S. Van Doorslaer, B. U. W. Maes, *Org. Lett.* **2016**, *18*, 2808–2811.
- [20] M. Tiemann, E. Nawrotzky, P. Schmieder, L. Wehrhan, S. Bergemann, V. Martos, W. Song, C. Arkona, B. G. Keller, J. Rademann, *Chem. Eur. J.* **2022**, *28*, e202201282.
- [21] a) S.-C. Cheng, G.-G. Chang, C.-Y. Chou, *Biophys. J.* **2010**, *98*, 1327–1336; b) B. Goyal, D. Goyal, *ACS Comb. Sci.* **2020**, *22*, 297–305; c) N. T. Nashed, A. Aniana, R. Ghirlando, S. C. Chiliveri, J. M. Louis, *Commun. Biol.* **2022**, *5*, 160; d) A. Kovalevsky, L. Coates, D. W. Kneller, R. Ghirlando, A. Aniana, N. T. Nashed, J. M. Louis, *J. Mol. Biol.* **2022**, *434*, 167876; e) A. Paciaroni, V. Libera, F. Ripanti, A. Orecchini, C. Petrillo, D. Francisci, E. Schiaroli, S. Sabbatini, A. Gidari, E. Bianconi, A. Macchiarulo, R. Hussain, L. Silvestrini, P. Moretti, N. Belhaj, M. Vercelli, Y. Roque, P. Mariani, L. Comez, F. Spinozzi, *Int. J. Mol. Sci.* **2023**, *24*, 6062.
- [22] a) A. Brik, Y.-C. Lin, J. Elder, C.-H. Wong, *Chem. Biol.* **2002**, *9*, 891–896; b) L. V. Lee, M. L. Mitchell, S.-J. Huang, V. V. Fokin, K. B. Sharpless, C.-H. Wong, *J. Am. Chem. Soc.* **2003**, *125*, 9588–9589; c) C.-Y. Wu, C.-F. Chang, J. S.-Y. Chen, C.-H. Wong, C.-H. Lin, *Angew. Chem. Int. Ed.* **2003**, *42*, 4661–4664; d) A. Brik, J. Muldoon, Y.-C. Lin, J. H. Elder, D. S. Goodsell, A. J. Olson, V. V. Fokin, K. B. Sharpless, C.-H. Wong, *ChemBioChem* **2003**, *4*, 1246–1248; e) S.-G. Lee, J. Chmielewski, *Chem. Biol.* **2006**, *13*, 421–426; f) K. B. Sharpless, R. Manetsch, *Expert Opin. Drug Discovery* **2006**, *1*, 525–538; g) Z. Li, Y. Wu, S. Zhen, K. Su, L. Zhang, F. Yang, M. A. McDonough, C. J. Schofield, X. Zhang, *Angew. Chem. Int. Ed.* **2022**, *61*, e202211510.
- [23] M. T. Marty, A. J. Baldwin, E. G. Marklund, G. K. A. Hochberg, J. L. P. Benesch, C. V. Robinson, *Anal. Chem.* **2015**, *87*, 4370–4376.
- [24] G. Wolber, T. Langer, *J. Chem. Inf. Model.* **2005**, *45*, 160–169.
- [25] S. C. Pan, B. List, *Angew. Chem. Int. Ed.* **2008**, *47*, 3622–3625.

Manuscript received: November 27, 2023

Accepted manuscript online: January 21, 2024

Version of record online: January 31, 2024